Nanoscale Photocurrent Variations at Metal-Modified Semiconductor Surfaces

ARTICLE *in* THE JOURNAL OF PHYSICAL CHEMISTRY B · JULY 1998

Impact Factor: 3.3 · DOI: 10.1021/jp9816420

2 AUTHORS, INCLUDING:

D. Meissner
Tallinn University of Technology
129 PUBLICATIONS **5,250** CITATIONS

NANOSCALE PHOTOCURRENT VARIATIONS AT METAL MODIFIED SEMICONDUCTOR SURFACES

R. HIESGEN, D. MEISSNER

Forschungszentrum Jülich, Institut für Energieverfahrenstechnik, D-52425 Jülich, Germany

e-mail: r.hiesgen@fz-juelich.de, d.meissner@fz-juelich.de

Abstract--The photocurrents measured by a scanning tunneling microscope have been used to analyze the electronic properties of nanoscale modified WSe_2 semiconductor surfaces. On uncovered crystals in ambient air space charges along steps can be analyzed. On copper modified semiconductor surfaces the space charge zones around pulse deposited metal particles and their dependence on the size of the metal particle can be determined and provide a first direct proof of size dependent barrier heights of nano-sized Schottky contacts. Also, the time evolution of the electronic properties of a metal modified WSe_2 surface under corrosion conditions was followed by photocurrent measurements. Combining photocurrent measurements and local current-/voltage curves the influence of recombination and of charges on the photocurrent can be separated.

Introduction

Since the semiconductor technology aims at using nanosized quantum structures, the electrical characterization also requires a resolution of such small dimensions. Nowadays, since the pioneering work by Rohrer and Binning [1] in the 80`s the necessary tools exist with the scanning tunneling microscopy (STM) and its related techniques like atomic force microscopy (AFM) [2] to measure the various properties of materials even down to the atomic scale.

In semiconductors it is possible to generate electron-hole pairs by exposure to light with wavelengths exceeding the bandgap of the material. These electron-hole pairs can be separated in an electric field and measured as a photovoltage or a (primary) photocurrent. Electric fields are formed when upon contact formation the electrochemical potentials of different materials equilibrate by a net charge flow from one material to the other. This happens at all types of semiconductor contacts e.g. at the Schottky junctions of metal/semiconductor contacts, at p/n-diodes or also at a surface of a semiconductor coupled capacitively to a counter electrode. Here, the bulk semiconductor and an adsorbate can also adjust their Fermi levels and lead to a surface photovoltage, which has been studied e.g. by STM already in 1990 [3]. Bringing a STM tip close to a semiconductor surface a metal-insulator-semiconductor (MIS) contact is formed. This has been first reported by Bard et al. [4] and investigated in more detail in our own measurements [5]. Under illumination a surface photovoltage is produced, the light induced charge carriers tunnel to the tip and are measured as a contribution to the tunneling current. The magnitude of the photocurrent is sensitive to the local electrical properties of the semiconductor and is influenced e.g. by the flat band potential, the band bending or the recombination rate. Therefore, the spatially resolved measurement of the photocurrent allows to determine the local electrical properties of the semiconductor. For example, we will show that local changes of the energy bands induced by metal particles of different sizes can be studied hereby. This is of interest e.g. for understanding the catalytic

influence of nanosized metal particles (**m**ultiple **n**ano **c**ontacts: MNC) on the electron transfer in electrochemistry or photoelectrochemistry [6,7]. Measurements of photocurrents with a STM have been reported mostly with the semiconductor being biased externally [9-13]. However, for the investigation of semiconductors for use in photovoltaics, the measurement of the short circuit photocurrent is more relevant since it minimizes the influence of photoconductivity on the measured current. Before our own investigations [5, 14-16] a spatially resolved short circuit photocurrent image has first been published in [17].

Experimental Section

With our setup which is based on a commercial STM (Nanoscope III, Digital Instruments, Santa Barbara, CA.) we are able to measure the topographical image of the semiconductor surface together with the spatially resolved photocurrent image. Here, the short circuit photocurrent can be recorded directly, but it is also possible to apply a voltage during the photocurrent measurement. In principle the photocurrent images are recorded as follows: the first scan line leading to the topographical surface image is measured in the dark in constant current mode under feedback control. Here, the sample is biased in forward direction to enable a sufficiently high dark current to flow which then becomes limited by the tunneling process between tip and surface. Only under this condition the path of the tip will represent the profile of the sample surface. This such recorded line profile is stored also as part of the topographical image. In the next scan line the tip follows the stored profile over the surface with the feedback control switched off. During this scan the bias voltage can be set to any value, e.g. to zero voltage where the short circuit current is recorded. Under illumination charge carriers are now generated in the semiconductor and can be measured as a tunneling current to the STM tip. By repetition of this scanning procedure an image of the surface structure (first line scans) and an image of the local photocurrent through the same area (second

line scans) is obtained simultaneously. The technique has been described in detail in [14].

Here it was also shown that the magnitude of the short circuit photocurrent does within certain limits not depend on the distance between the tip and the semiconductor sample. For the appropriate tip distances the photocurrent is only determined by the properties of the semiconductor and not limited by the tunneling process. The system consisting of the metal tunneling tip, the gap and the semiconductor behaves perfectly as a MIS solar cell [5]. Corresponding results have meanwhile also been reported in [18]. Therefore changes of the tunneling gap do not change the measured photocurrent.

Experiments have been performed in ambient air, in dry nitrogen atmosphere and in electrolyte under potentiostatic control. In this paper only results measured in ambient air will be reported for which an adsorbed water film on the surface is assumed (compare also [19]). For illumination a 5 mW He/Ne-Laser (Uniphase, Starna GmbH, Pfungstadt, λ = 653 nm) has been used without further focussing. The illuminated area beneath the tip is about 1 mm^2 and the illumination is performed with an incident angel of about 70^o. Influences of shadowing of the surface by the tip could not be detected. Additionally it was confirmed that the photocurrent increases linearly with the light intensity.

As model semiconductors n- and p-type WSe_2 monocrystalline samples with doping levels of $4 \cdot 10^{16}$ cm^{-3} have been used. These layered semiconductors can be cleaved with adhesive tape exposing large terraces of non-reactive van-der-Waals surfaces separated by only few monolayers high steps. An ohmic back contact has been prepared by soldering indium to the back of the crystal and has been verified by current/voltage-measurements. The voltage values given are always those of the semiconductor with respect to the metal STM tip which is connected to ground.

Results and Discussion

Current/Voltage Curves

In Fig. 1 the dark and illuminated current-/voltage curves measured on a n-type WSe_2 surface are shown. In the dark the current-/voltage curve exhibits a diode behavior with no detectable current flowing at short circuit and under reverse bias conditions. The diode behavior reflects the sharing of the externally applied voltage into a voltage drop across the tunneling gap and that across the space charge region of the semiconductor. Therefore the voltage drop across the space charge region of the semiconductor changes with the applied voltage leading to a change of the barrier height for majority carriers within the semiconductor. Under illumination only the photocurrent contributes to the tunneling current in this voltage range and is measured in the photocurrent image. A short circuit photocurrent of 0.7 nA is obtained and the open circuit voltage is about –500 mV. It can be seen in the I/V-curve under illumination that the photocurrent does not saturate at more positive voltages but is further increasing. As demonstrated in Fig. 1 this rise can be fitted to the Gärtner equation [20] as was already shown in [5]. The reason is that the depletion region at the surface where minority carriers are collected is smaller than the penetration depth of the light. This leads to an increase of the collected current with the square root of the applied voltage reflecting the increasing thickness of the space charge layer. From fitting the rising part of the measured photocurrent curve to the Gärtner equation the flat band potential U_{fb} can be derived as will be used below.

Space Charge Regions along the Surface

In Fig. 2 a measurement of the topography together with the short circuit photocurrent recorded on n-WSe_2 is shown. The topography image is depicted in Fig. 2a with a lower (dark) to higher (light) areas gray scale. Terraces separated by diagonal step lines consisting of two atomic layers down and two layers up can be seen on the surface. In

Fig. 2b the corresponding short circuit photocurrent is shown. In the images only the photocurrent differences are shown. Larger photocurrents show up in the image as brighter areas. Along the steps visible in the topographical image in Fig. 2a and the zoomed in image in Fig. 3a the photocurrent, shown in Fig. 2b and Fig. 3b, is increased. The zones of slightly decreased photocurrents on both sides can be seen more clearly in a current profile of the step as given in Fig. 3c. The zone of enhanced photocurrent is 175 nm wide and the total photocurrent increases here by about 50 %.

Fig. 2c shows an image of the photocurrent measured on the same area as in Fig. 2b but recorded with an applied voltage of +1 V in reverse direction. The zones of enhanced photocurrent along the steps have widened significantly. The width has increased from 175 nm under short circuit conditions to 580 nm as can be seen in the current profile in Fig. 3e recorded along the line drawn in the photocurrent image of Fig. 3d.

Corresponding results showing an inverse behavior have been obtained on p-WSe_2. Fig. 3 f and h show a short circuit photocurrent image and a current profile across the step shown in the topographical image in Fig. 3g. The effect is smaller than in the n-type crystal: the zone of decreased photocurrent is only 50 nm wide and the current is reduced by only 20 %. The zone of increased current measured at the step on the n-type crystal is replaced by one of decreased current surrounded this time by a region of larger photocurrent.

Our model explaining these results is given in Fig. 4 showing on an energy scale the position of the bottom of the conduction band and the top of the valence band along the semiconductor surface below a schematic drawing of the illuminated surface with a negative charge trapped at a step. Probably due to electrons tunneling to the semiconductor, surface states which are very likely to be formed at the step sites are charged negatively. These negative charges cause an upward shift of the position of the energy bands at the location of the steps. For an n-type crystal the resulting change of the electric fields inside the semiconductor leads to a decrease of the number of electrons

(majority carriers) and an increase of the number of holes (minorities) reaching the surface. Hereby the magnitude of the minority carrier, i.e. hole, photocurrent measured at the steps increases. For the p-type crystal the situation is different. Here now electrons are the minority carriers and are accumulated at the interfaces and the corresponding upward shift of band edges should lead to a decreased photocurrent. The analysis of the Schottky barrier height at the surface of n-WSe_2 in ambient air has resulted in values of about 1 eV [5]. The barrier height at the p-WSe_2 can be estimated from the difference between the bandgap of 1.2 eV and the barrier height on the n-doped crystal. With an expected value of about 0.2 eV it is significantly smaller than on n-type material which leads to much higher charge carrier recombination rates, smaller charging and therefore smaller flat band potential shifts.

Corrosion Processes

In Fig. 5 a sequence of three measurements of the topography (left side) together with the corresponding short circuit photocurrent (right side) on n-WSe_2 is presented showing an evolution of the height and the photocurrent distribution with time due to corrosion processes in ambient environment within a period of 180 minutes. During this time the surface was continuously scanned by the STM and many images were recorded. The topographical and the photocurrent images have all the same scan area and are shown with the same contrast: a height difference of 7 nm from black to white in the surface pictures and a current difference of 200 pA from black to white in the photocurrent images. All structures on the images are shifting to the upper left with time due to a slow drift of the sample.

Fig. 5a is taken just after applying a voltage pulse of +7 V during one second to the copper tip in order to deposit some copper particles onto the semiconductor surface. Besides the deposition of particles this results in a hole in the upper left corner of the

image. From there some defect lines with a height of only about 0.1 nm start across the image. They are obviously caused by the voltage pulse which has produced mechanical distortion in the crystal. Also a number of particles of different sizes, most probably copper from the tip, have been deposited onto the surface as, e.g., in the lower half of the image. The corresponding short circuit photocurrent image reveals strong photocurrent modulations around the hole and at all three copper particles seen here. At most photocurrent depletion regions there is still a photocurrent measurable. However, the current vanishes completely near to the two copper clusters 1, 2, and 4 in the lower middle. These two copper clusters are both consisting of three agglomerated but still distinguishable copper particles, each. However, two smaller copper particles (3 and 5) located in the bottom part of the image are producing an increased photocurrent. These two types of behavior have been observed on many different images for copper deposited on n-WSe_2 with increased photocurrents being observed only in few cases. For noble metal deposits only decreased photocurrents have yet been observed. We therefore take the increase of photocurrent at copper particles as a yet not understood exemption possibly due to charging of oxidized copper.

The measurement shown in Fig. 5b has been performed 40 minutes later. Two of the defect lines have moved in the meantime and are now attached to the neighboring copper particles. The easy movement of these defect lines is probably due to the fact that they are formed by only a slight displacement of the surface atoms obviously produced by the stress of the defect formation. From each of the three copper clusters (1, 2 and 4) copper particles have vanished probably due to a removal by the scanning tip. The contrast in the photocurrent image is weaker now. Measurements of the current at all three corresponding dark spots show that there is no decay of the current to zero any more. This will be analyzed in more detail in the next chapter.

Fig. 5c is taken 180 minutes after Fig. 5a. Here, the surface has changed further. The straight defect lines seen in the two previous images have vanished. They are replaced

by three 2 nm deep grooves in the surface with a width of 30 nm forming additional branches to the sides. These grooves follow more or less the former path of the defect lines. In some parts they have taken a different way across the surface, but they are still pinned to the copper particles at the surface. The evolution of these corrosion grooves is obviously connected to the defects lines seen in the beginning. They seem to be influenced by electric fields in the surface which cause variations in the photocurrents across the surface, all induced by the initial mechanical stress and/or the deposited copper particles. Already in the photocurrent image of Fig. 5b the curved structure of higher photocurrent between particles 1, 2 and 4 seems to resemble closely but not exactly the path of the final corrosion groove in the topographical image of Fig. 5c. It indicates that the final pathway of the corrosion grooves can be estimated to some extent beforehand from the photocurrent image taken from the still intact surface. This certainly needs further investigation. However, here STM photocurrent imaging may find a further application, even if surface field analysis using this technique still faces several problems.

In Fig. 6 the origin of the photocurrent image is analyzed in more detail. Here, a topographical image taken 220 minutes after the first scan is shown. The image stored contains a square grid of 32 by 32 points across the surface on which current-/voltage curves have been recorded under illumination while scanning the image. Three of these current-/voltage curves measured at different sites on the surface (marked by arbitrary numbers) are chosen for a more detailed analysis. In order to discuss the different current-/voltage curves a few characteristic values have been derived from the curves and have been summarized in table 1.

Most of the current-/voltage curves taken under illumination do not show the behavior expected for an ideal photodiode, i.e. a voltage independent photocurrent is added to the dark current. Typically, the rise of the photocurrent starts only after applying a certain overvoltage defined here as the potential difference between the onset of the cathodic forward current and the onset of the photocurrent leading to a s-shaped I/V-curve. This

is attributed to a high rate of recombination at the surface when the band bending is small. As a measure of the width of this recombination region for practical reasons the voltage difference between the half-wave potential of the photocurrent rise ($U_{1/2}$) and the potential of the onset of the cathodic current ($U_{(Id=0)}$) has been taken and given as ΔV in table 1.

As reported before [5], the photocurrent follows a Gärtner equation after saturation. All curves were fitted using this equation and the flat band potential has been determined from this fit and is given as U_{fb}. Additionally, the short circuit current I_{sc} and the magnitude of the photocurrent I_{1500} measured 1500 mV positive of the flat band potential have been derived from the curves. The value I_{1500} allows to estimate the saturation photocurrent even if there is still a slight increase due to the Gärtner behavior. Differences in this value reflect differences in collection efficiency, for example a different width of the space charge region at this location.

The I/V-curve at location "1" as given in Fig. 6b is typical for an undisturbed part of the surface. Here, the recombination region of the I/V-curve is small compared e.g. to the I/V-curve taken at point "2", which is directly located at one of the grooves formed by the corrosion of the semiconductor surface. The rise of the photocurrent, expressed by the half-wave potential, is shifted so far positive that under short circuit conditions the photocurrent is still diminished by recombination. In addition, the rise of the photocurrent is a bit less steep at location "2" than that of the two other curves leading to the smallest "saturation" photocurrent of the three examples discussed here.

The current-/voltage curve measured at location "3" is taken above one of the copper particles deposited onto the semiconductor. Although the I/V-curve is measured on a metal particle it shows the same diode behavior as all other curves. Taking this into account it is obvious that the current is controlled by the semiconductor/metal interface and not by the tunneling from the metal particle to the metal tip. In this I/V-curve no recombination region occurs. The photocurrent is rising from the onset of the cathodic

current. Although this value is more positive in curve 1 than in the ideal curve 3 both curves are identical in the forward current more negative than -570 mV and also at potentials more positive than –140 mV. They only differ in the dip of the recombination region seen in curve 1 which is demonstrated in Fig 6e where curves "1" and "3" are plotted together. Therefore also the values for the flat band potential and the short circuit photocurrent are quite close and not distinguishable within the range of the experimental errors, whereas the value for the flat band potential at location "2" is significantly more negative. Since the cathodic currents are identical it can be concluded that the voltage drops over the tunneling gap and therefore the tunneling distances are the same for both locations and only the recombination rate is different. The recombination is obviously diminished by the semiconductor/metal interface.

In the three current-/voltage curves discussed above two different reasons for the reduction of the short circuit photocurrent imaged in figures 2, 3 and 5 can be distinguished. At the corrosion grooves large recombination regions can be found connected to a smaller collection efficiency of the photocurrent. On the other hand the presence of a copper particle obviously reduces the surface recombination leaving the "saturation" photocurrent unchanged.

In Fig. 7 two topography/photocurrent measurements are shown taken at the same area as in Fig. 5. In Fig. 7a the photocurrent has been measured under short circuit conditions and in Fig. 7b a voltage of +500 mV in reverse direction has been applied during photocurrent recording. The broad dark area between the copper particles which can be seen in Fig. 7a has vanished completely in Fig. 7b. Here due to the applied reverse bias the space charge regions have grown considerably which leads to a higher collection of the photocurrent from deeper regions of the crystal. Therefore the influence of the surface is smaller here. Taking this into account it can be concluded that the reduction of the photocurrent takes place predominantly at the surface and is caused by surface recombination or surface potential differences. On the other hand, when the photocur-

rent is collected from deeper layers also structures in the bulk start to influence the photocurrent. Since the long range structures in Fig. 7b become more pronounced here compared to the short circuit photocurrent image they are probably caused by electric fields inside the crystal.

Contact Size Effects

As indicated already above, by accident the sample allows also to study the influence of the size of the copper particles in more detail. In Figures 8 to 11 a more detailed investigation of cluster 2 in Fig. 5 is given. In the topographical image of Fig. 8 an early height profile measured along the line is plotted together with the enlarged surface image of the cluster from Fig. 5a. Three connected particles can be seen. They exhibit heights of about 3 nm and are about 40 nm wide. The whole agglomerate has a diameter of about 70 nm. In the short circuit photocurrent image also a current profile measured along the same line is given. The photocurrent is reduced not only directly at the position of the metal particles but in a region of 160 nm in diameter which is more than double the width of the whole cluster. Directly below the particles there is an additional reduction of the current detectable. This reduction has the same diameter of 40 nm as the particle itself and here, the current drops down to zero as can be seen in the current profile.

In Fig. 9 this cluster is imaged again after further scanning for 3 hours. Thereby two of the three copper particles have been removed and only the biggest one still remained. The profile along the line shows the dimensions of one single copper particle with a height of about 3 nm and a diameter of 40 nm as before. However, there no agglomerate exists anymore. Now a reduction of the photocurrent is only recorded directly below the particle as can be seen in the current profile plotted into the short circuit photocurrent image. No further influence on the neighboring areas can be seen here. Also the photocurrent below the particle does not drop to zero anymore. As discussed above corre-

sponding results were obtained also for other agglomerates of copper particles on this as well as on other samples.

These results can be explained perfectly by a model first suggested by Noshaka, Norimatsu and Miyama [6] and evaluated in detail by Tsubomura, Nakato and their group [7] assuming an influence of the size of the metal particles on the energy bands of the semiconductor and the contact properties. However, there has not been any direct proof of this model yet. Here now we finally present direct experimental evidence for the predictions of their model: The extension of the space charge region at the semiconductor/metal interface depends on the size of the contact area and it is not fully developed for small particles laterally as well as into the semiconductor which leads to the development of an "effective barrier" [7].

No published results have been found on direct measurements of the barrier height for copper on n-WSe_2. Its barrier height on the n-type semiconductor has been estimated from measurements on p-WSe_2 [21] to be about 0.2 eV which means the contact should be nearly ohmic. The Schottky barrier on the unmodified neutral surface of the n-WSe_2/water interface has been determined to about 1 eV [5] which means that copper leads to a pronounced reduction of the barrier below the copper with respect to the surrounding water film covered semiconductor.

A scheme of the course of the energy band edges from the surface into the semiconductor at the unmodified surface is given in Fig. 10a. It shows the situation under illumination where the Fermi level is split into the quasi Fermi levels of the electrons ($E_{F,n}$) which is almost unchanged by the illumination and of the holes which are the minority carriers ($E_{F,h}$). The positions of the band edges at the semiconductor surface are marked by $E_{c,s}$ for the bottom edge of the conduction band and $E_{v,s}$ for the top edge of the valence band. The splitting of the quasi Fermi levels at the surface is a measure for the produced photovoltage. Below a big copper particle the barrier height between copper and the n-WSe_2 is significantly smaller than at the uncovered surface. The course of the

band bending inside the crystal at this position is shown in Fig. 10b. The positions of the band edges at the surface are called here $E_{c,m}$ and $E_{v,m}$ for the conduction and valence bands, respectively. There is no Fermi level splitting drawn in this case because no photocurrent at all has been measured directly below the big copper cluster. This lack of photocurrent at the metal/semiconductor interface is definitely not caused by shadowing of the light by the metal itself as was found in many experiments and is again demonstrated by the difference between Figures 8 and 9.

The positions of the conduction and valence band edges along the surface across a big copper cluster are plotted in Fig. 10c. Below the copper cluster the band edges are lowered with a smooth rise besides the metal reaching the band positions of the uncovered surface only in a certain distance from the copper particle (compare Fig. 8). As a result at the copper particles there is a fully developed space charge region along the surface exceeding the dimensions of the metal. This situation is indicated schematically in Fig. 10d. In the current image this space charge region has an extension of 40 to 60 nm measured from the edge of the copper particle to the point where the current reaches the value of the uncovered surface. Using equation 1 taken from [22] with

$$d_s = \left(\frac{\varepsilon \varepsilon_0 V_0}{2\pi e N_A} \right)^{\frac{1}{2}} \qquad (1)$$

and the nominal doping level of our sample of $N_A = 5 \cdot 10^{16}$ cm^{-3} a space charge width d_s of 40 nm can be calculated which is in agreement with the measured values. The other parameters used have been $V_b = 0.8$ V, and $\varepsilon = 7.3$ [22].

If the metal particle is small the situation may be quite different according to the model of Nakato and Tsubomura. In Fig. 11a a sketch of the course of the energy bands reaching into the semiconductor is shown for this case. The position of the conduction- and valence band edges at the point contact between metal and semiconductor, marked as $E_{c,m}$ and $E_{v,m}$, are the same as for a big particle but the metal is assumed to influence

the semiconductor not enough to change the position of the band edges along the whole space charge region inside the semiconductor. As a result the bands are bent down only at the surface below the metal but are mostly unchanged inside the crystal. This results in the formation of an "effective barrier" with a height depending on the size of the contact (compare [7]). The resulting course along the surface than looks like that in Fig. 11b and results in a smaller band bending for the majority as well as for the minority carriers. Only directly below the copper the position of the band edges has changed but there is no extended space charge region existing around the metal as is indicated in the scheme of Fig. 11c. This is exactly what we found in the measurement. As can be seen in Fig. 9 the current is only diminished directly below the small particle with no influence on the neighboring semiconductor.

At the metal the barrier for majority carriers is higher than behind the big metal particle which therefore diminishes the number of majority carriers reaching the surface i.e. the loss currents. The small barrier for the minority carriers formed this way influences the photocurrent only very little because the minority carriers are collected at the surface due to the electric field in the space charge zone. At those small metal particles the surface recombination should be reduced thereby. This explains the experimental result that the photocurrent below the small copper particle is not reduced to zero as it is below the big cluster. With this model also the ideal behavior of the I/V-curve measured at a single metal particle in Fig. 6d can be explained. Also here the decrease of surface recombination leads to the absence of any recombination region in the I/V-curves.

Nakato and Tsubomura had developed their model to explain unusually high open circuit voltages using small platinum particles on n-Si [2, 23]. However, here the non metal parts of the surface are oxidized leading to blocking semiconductor/oxide/electrolyte contacts. In real photoelectrochemical experiments metal (gold and Pt) point contacts on p-GaAs (**M**ultiple **N**ano **C**ontacts) have been found to significantly decrease the overvoltage necessary to drive a reaction at the semiconductor surface without increas-

ing the loss currents as it occurs when extended semiconductor/metal contacts are used or the surface is covered by metal surface states [8, 24]. In both cases the experiments were explained using "effective" Schottky barriers instead of the values found for a complete coverage of the surface by the metals used. However, these interpretations were only based on measurements integrating over the entire interface area. A direct visualization of the differences in space charge regions due to the influence of differently sized metal particles was not possible at that time. The results described here therefore provide a first direct proof that the model used to describe the microscopic properties at the semiconductor interface correctly.

Conclusions

We have shown that the spatially resolved photocurrent is a sensitive tool for analyzing the electronic variations on a semiconductor surface. Variations in flat band potential as well as changes in the recombination rate can be detected and linked to structures of the surface, below the surface, or to metal particles modifying the surfaces. It is possible to visualize the space charge regions along steps as well as around catalyst particles on the surface and to follow the electronic changes caused by corrosion. In combination with locally measured current-/voltage curves the different influences of recombination and of charging effects can be separated. Information can be derived not only from the very surface but also from sub-surface layers by applying a bias voltage during photocurrent recording. Measuring the photocurrent made it possible to directly observe effective barriers of copper particles and of size effects influencing the width of the space charge layer at the surface. Thereby a model suggested already in 1984 was finally confirmed.

Acknowledgements

We thank Prof. Dr. Rüdiger Memming, Hamburg, as well as all members of our group for valuable discussions. Financial support by the Volkswagen Foundation under contracts No. I/72 365, I/71 902 and by the Deutsche Forschungsgemeinschaft under contract No. ME 855/3-1 is gratefully acknowledged. We thank Prof. Levy, EPFL Lausanne, Prof. Lux-Steiner, Dr. Alonso-Vante and Y. Tomm, HMI Berlin, for providing semiconductor samples.

References

1. Binning, G.: Rohrer, H. *Helv. Phys. Acta* 1982, **55**, 726.

2. Binning, G.: Quate, C. F.: Gerber, C. *Phys. Rev. Lett.* 1986, **56**, 930.

3. Hamers, R.: Markert, K. *Phys. Rev. Lett.* 1990, **64**, 1051.

4. Fan, F. R. F.: Bard, A. *J. Phys. Chem.* 1993, **97**, 1431 - 36.

5. Hiesgen, R.: Meissner, D. *Electrochimica Acta* 1997, **42**, 2881.

6. Nosaka, Y.: Norimatsu, K.: Miyama, H. *Chem.. Phys. Lett* .1984, **106**, 128.

7. Nakato, Y.: Ueda, K.: Yano, H.: Tsubomura, H. *J. Phys. Chem.* 1988, **92**, 2316 and references cited therein.

8. Maier, A.: Uhlendorf, I.: Meissner, D. *Electrochimica Acta* 1995, **40**, 10, 1523.

9. Akari, S.: Lux-Steiner, Ch. M.: Glöckler, K.: Schill, T.: Heitkamp, R. *Ann. Physik* 1993, **2**, 141 - 148.

10. Akari, S.: Lux-Steiner, M. Ch.: Vögt, M.: Stachel, M.: Dransfeld, K. *J. Vac. Sci. Technol. B* 1990, **9**, 561 - 563.

11. Qian, L. Q.: Wessels, B. W. *Appl. Phys. Lett.* 1991, **58**, 1295 - 1296.

12. Akari, S.: Friemelt, K.: Glöckle, K.: Lux-Steiner, M. Ch.: Bucher, E.: Dransfeld, K. *Appl. Phys. A* 1993, **57**, 221 - 223.

13. Qian, L. Q.: Wessels, B. W. Inst. Phys. Conf. Ser. No 117: Section 8, *Proc. of the Microsc. Semicond. Mater. Conf.*, Oxford, 1991, March 25-28.

14. Hiesgen, R.: Meissner, D. *Fres. J. Anal. Chem.* 1997, **358**, 54.

15. Hiesgen, R. *Proceedings of the 7th Workshop on Frontiers in Quantum Solar Energy Conversion Photovoltaics & Photoelectrochemistry*, Rauris, 1995, 12-18 March, 25 - 26.

16. Hiesgen, R.: Meissner, D. *Book of Abstracts of 60. Bunsenkolloquium*, Jena, 1995, July 12-14.

17. Kuk, Y.: Becker, R. S.: Silverman, P. J.: Kochanski, G. P. *Phys. Rev. Lett.* 1990,

65, 456-459.

18. Sommerhalter, Ch.: Matthes, Th. W.: Boneberg, J.: Leiderer, P. *J. Vac. Sci. Technol. B* 1997, **15**, 1876-1883.

19. Schaar-Gabriel, E.: Alonso-Vante, N.: Tributsch, H. *Surf. Sci.* 1996, **360**, 508.

20. Gärtner, W. W. *Phys. Rev.* 1959, **116**, 84-87.

21. Klein, A.: Pettenkofer, C.: Jaegermann, W.: Lux-Steiner, M.: Bucher, E. *Surf. Sci*. 1994, **321**, 19.

22. Schlaf, R.: Klein, A.: Pettenkofer, C.: Jaegermann, W. *Phys. Rev. B* 1993, **48**, 14242-14252.

23. Nakato, Y.: Tsubomura, H. *Electrochim Acta* 1992, **37**, 897.

24. Meier, A.: Uhlendorf, I.: Meissner, D. *Electrochim. Acta* 1995, **40**, 1523.

Figure Captions

Fig. 1 Typical current-/voltage curves measured with the STM in the dark and under illumination on n-WSe_2 terraces in ambient air. Tunneling parameters for distance control: I_{set} = 2 nA, U = -1 V. Characteristic values of the curves are: $U_{(I=0)}$): onset of the cathodic current, ΔV: recombination region, U_{fb}: flat band potential, $U_{1/2}$: half-wave potential of the photocurrent rise, I_{sc}: short circuit current, I_{1500}: photocurrent 1500 mV positive of the cathodic current onset.

Fig. 2 Topography and photocurrent images recorded on n-WSe_2:
a) STM image recorded with a setpoint current I_{set} = 1 nA at U = -1 V,
b) short circuit photocurrent,
c) photocurrent measured at +1 V in reverse direction

Fig. 3 Topographical- and photocurrent images in the vicinity of steps together with a current profile measured along the plotted lines for:
a) a step on n-WSe_2, I_{set} = 1 nA, U = -1 V,
b) short circuit photocurrent on n-WSe_2 and
c) recorded along the line shown in a,
d) photocurrent measured at +1V in reverse direction on the area shown in a,
e) corresponding photocurrent line scan,
f) STM image of a step on p-WSe_2, I_{set} = 1 nA, U = +1 V and
g) the corresponding photocurrent image,
h) photocurrent line scan.

Fig. 4 Schematic energy scheme of the positions of the bottom of the conduction band and the top of the valence band across a surface step under illumination. A negative charge is assumed to be located at the step and its influence on the majority carriers (electrons) and the light induced minority carriers (holes) is shown.

Fig. 5 Series of STM and simultaneously recorded short circuit photocurrent images taken in ambient air after pulse deposition of copper from a copper tip onto the surface of n-WSe_2:
a) directly after the voltage pulse,
b) after 40 minutes,
c) after 180 minutes

Fig. 6 a) STM image of corroded n-WSe_2 (same area as in Fig. 6) after 220 minutes of imaging,
b) current-/voltage curve taken under illumination on the undisturbed surface at the location marked at 1,
c) current-/voltage curve taken under illumination at a groove (location 2),
d) current-/voltage curve taken on a copper particle under illumination (location 3),
e) current-/voltage curve taken at position "1" together with that taken at position 3.

Fig. 7 STM together with the photocurrent images recorded on n-WSe_2 in ambient air:
a) short circuit photocurrent
b) photocurrent recorded at +500 mV in reverse direction.

Fig. 8 STM (left side) and short circuit photocurrent (right side) images of a copper cluster agglomerate on n-WSe_2 together with the height- and current profiles, respectively, measured along the given line.

Fig. 9 STM (left side) and photocurrent images recorded at +500 mV in reverse direction together with the height- and current profiles, respectively, measured along the given line across the same copper cluster as in Fig. 9 but after removal of the other clusters (and appearance of a default line, compare Fig. 5).

Fig. 10 Schemes describing the influence of Cu cluster agglomerates on the band edge profiles of n-WSe_2.
a) Energy diagram at the water / film interface and
b) profile below a big metal island,
c) energy diagrams of the band edges along the surface across the island and
d) x/z-scheme of space charge regions inside the semiconductor.
The directions x and z are used along and perpendicular to (i.e. into the bulk of) the semiconductor, respectively.

Fig. 11 Schemes as in fig 10 describing the influence of small Cu clusters.

Analysis of current-/voltage curves

	$U_{(Id=0)}$/mV	U_{fb}/mV	ΔV/mV	$U_{1/2}$/mV	I_{1500}/nA	I_{sc}/nA
1	-451	-630	200	-251	1,15	0,69
2	-560	-880	517	-43	1,07	0,61
3	-531	-520	-	-	1,13	0,65

$U_{(I=0)}$: onset of the cathodic current
U_{fb}: extrapolated flat band potential from Gärtner fit to the photocurrent
$U_{1/2}$: half-wave potential of the photocurrent onset
ΔV: $U_{1/2}$-$U_{(I=0)}$: extension of recombination region
I_{1500}: photocurrent at U = $U_{(I=0)}$ + 1500 mV
I_{sc}: short circuit photocurrent at U = 0 mV

Table 1

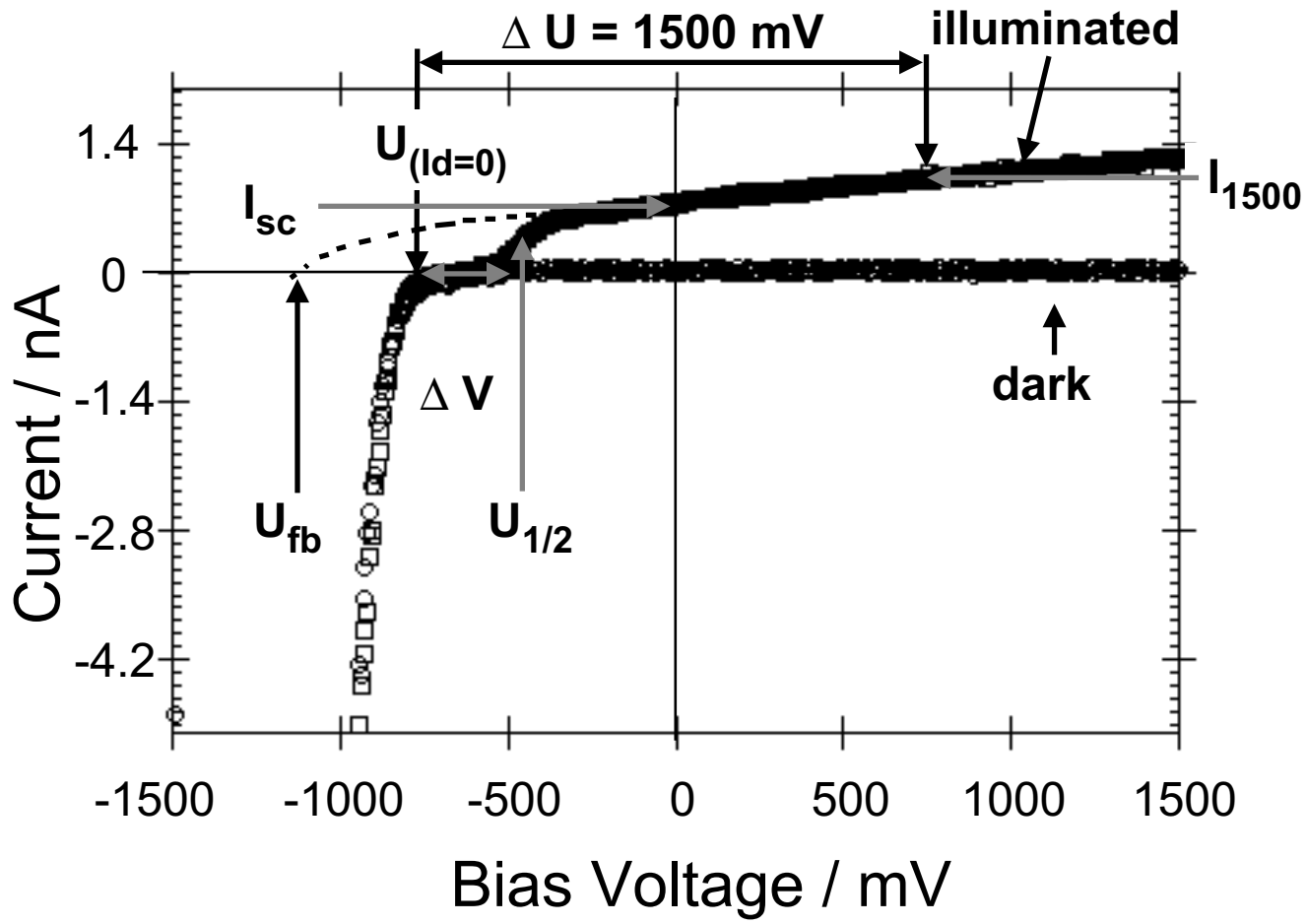
Δ U = 1500 mV
illuminated
U(Id=0)
Isc
I1500
dark
Δ V
Ufb
U1/2
1.4
0
-1.4
-2.8
-4.2
Current / nA
-1500
-1000
-500
0
500
1000
1500
Bias Voltage / mV

Fig. 1

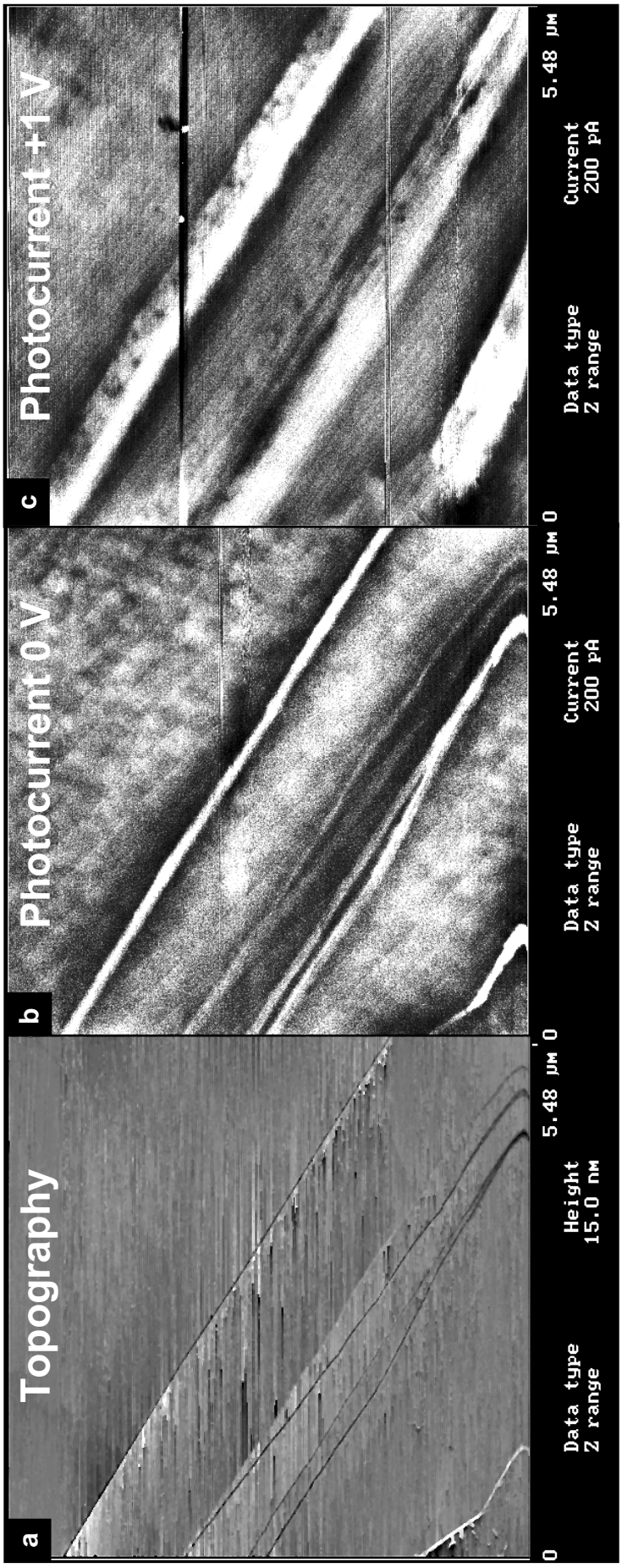
a
Topography
Data type
Z range
Height
15.0 nm
0
5.48 µm 0
b
Photocurrent 0 V
Data type
Z range
Current
200 pA
5.48 µm 0
c
Photocurrent +1 V
Data type
Z range
Current
200 pA
5.48 µm

Fig. 2

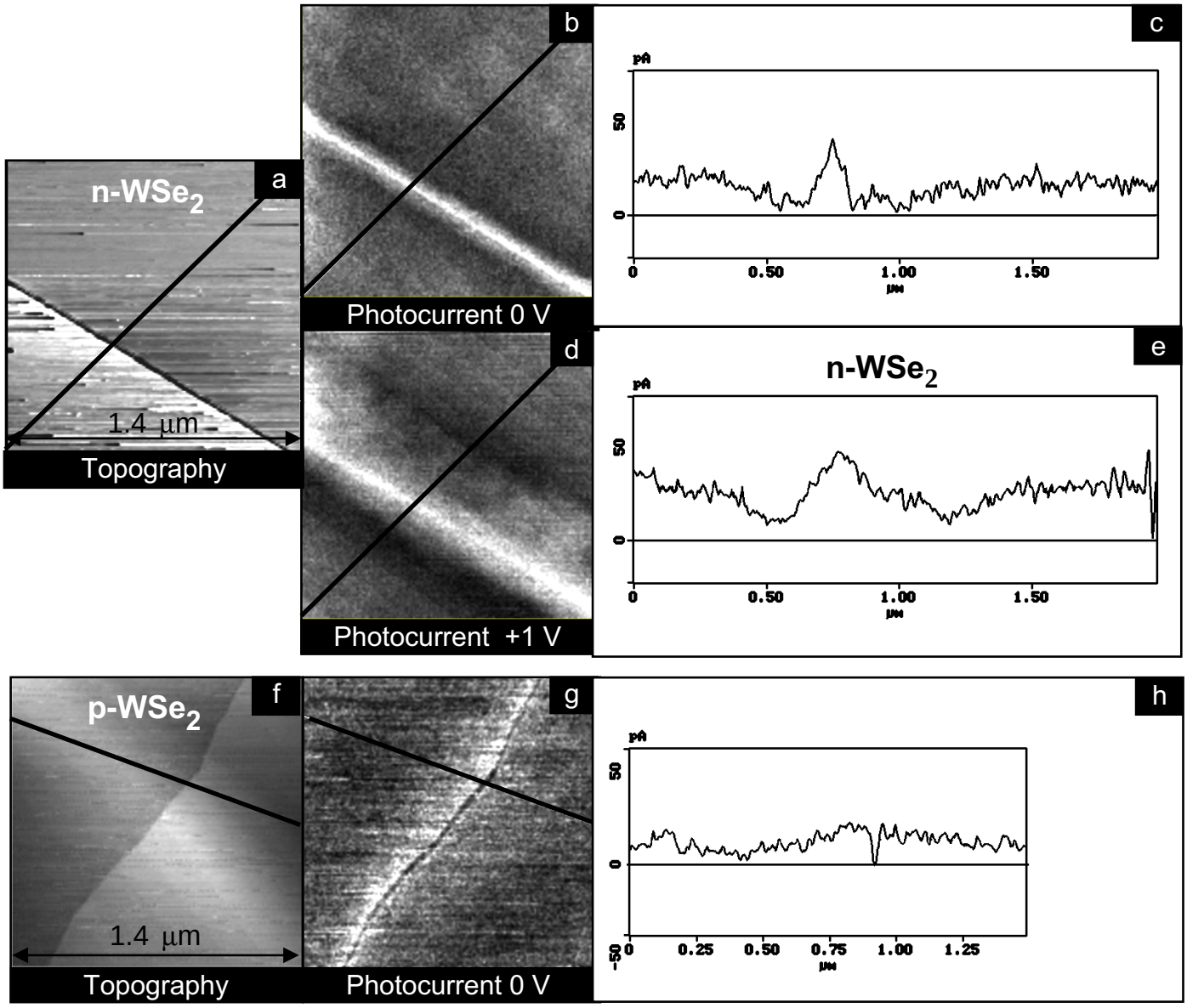
a
n-WSe2
1.4 µm
Topography
b
Photocurrent 0 V
c
pA
50
0
0
0.50
1.00
1.50
µm
d
Photocurrent +1 V
e
n-WSe2
pA
50
0
0
0.50
1.00
1.50
µm
f
p-WSe2
1.4 µm
Topography
g
Photocurrent 0 V
h
pA
50
0
-50
0
0.25
0.50
0.75
1.00
1.25
µm

Fig. 3

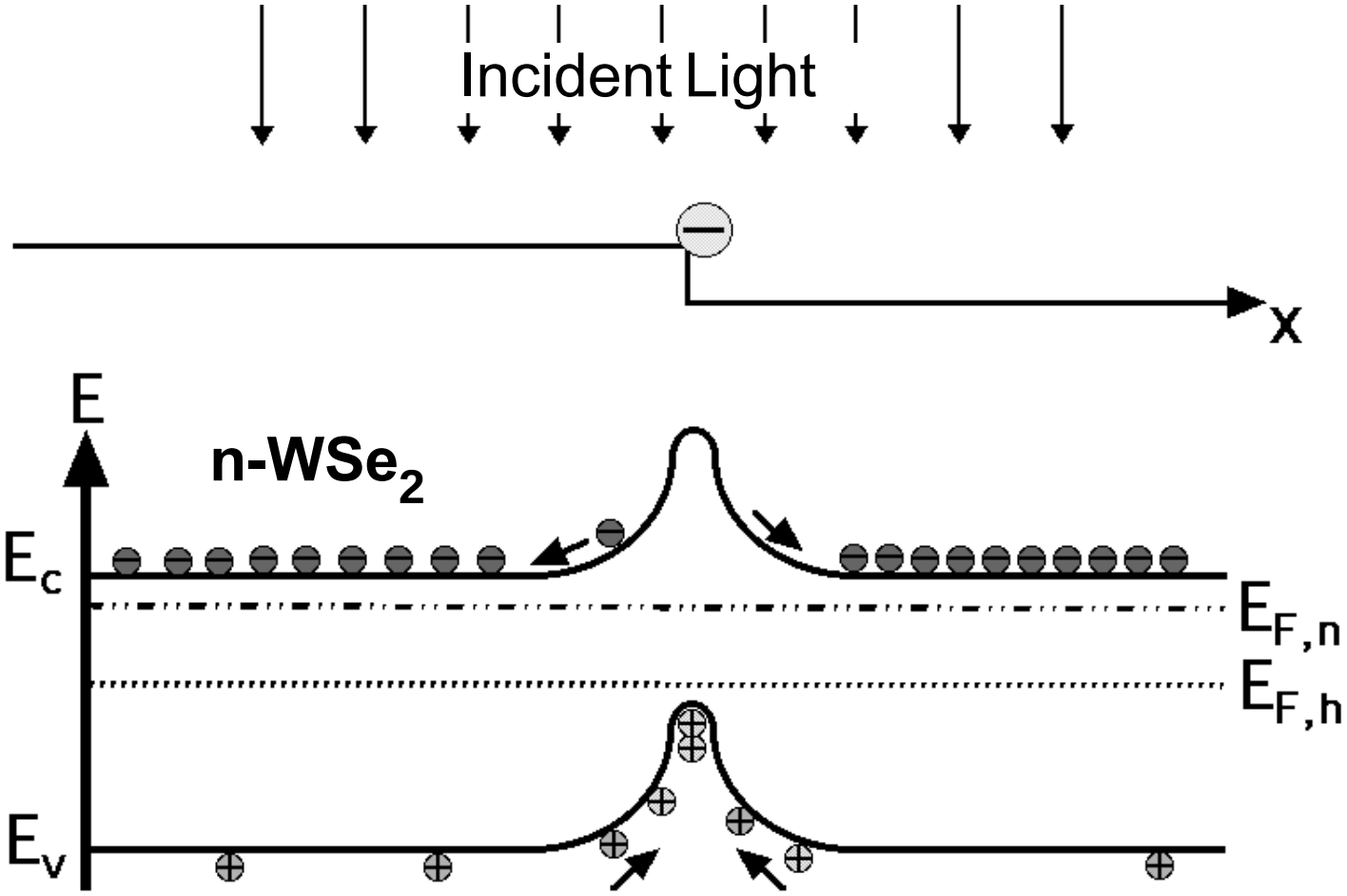

Fig. 4

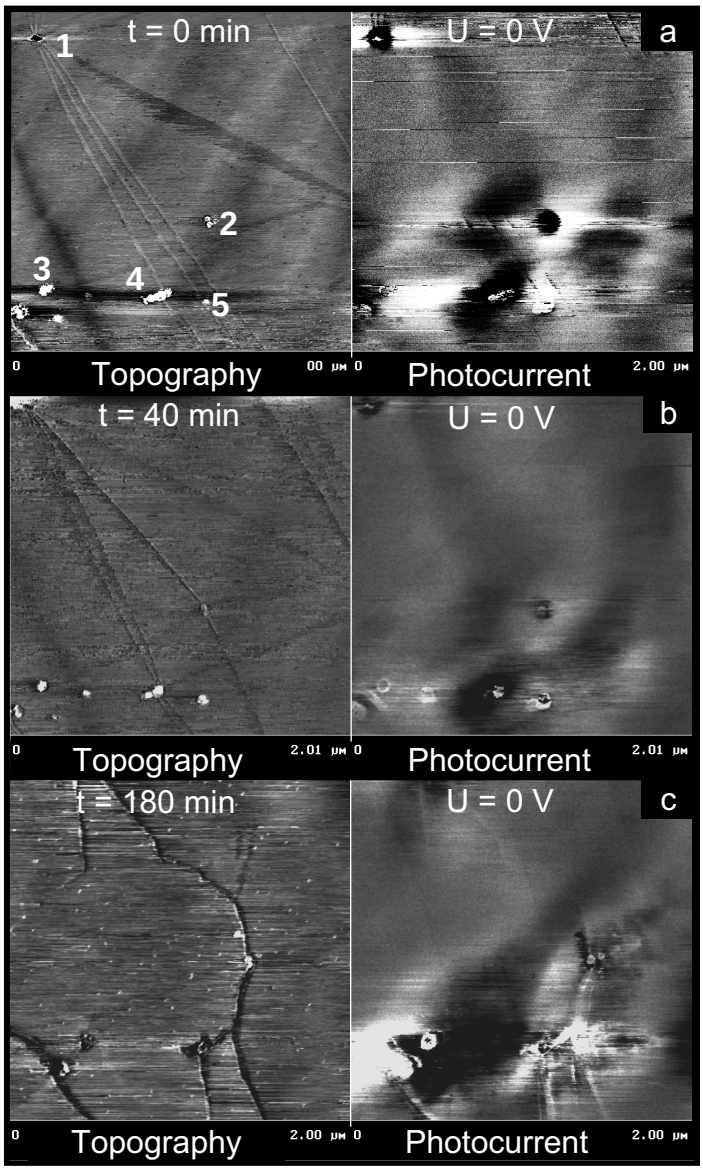
t = 0 min
1
2
3
4
5
U = 0 V
a
0
Topography
00 µm
0
Photocurrent
2.00 µm
t = 40 min
U = 0 V
b
0
Topography
2.01 µm
0
Photocurrent
2.01 µm
t = 180 min
U = 0 V
c
0
Topography
2.00 µm
0
Photocurrent
2.00 µm

Fig. 5

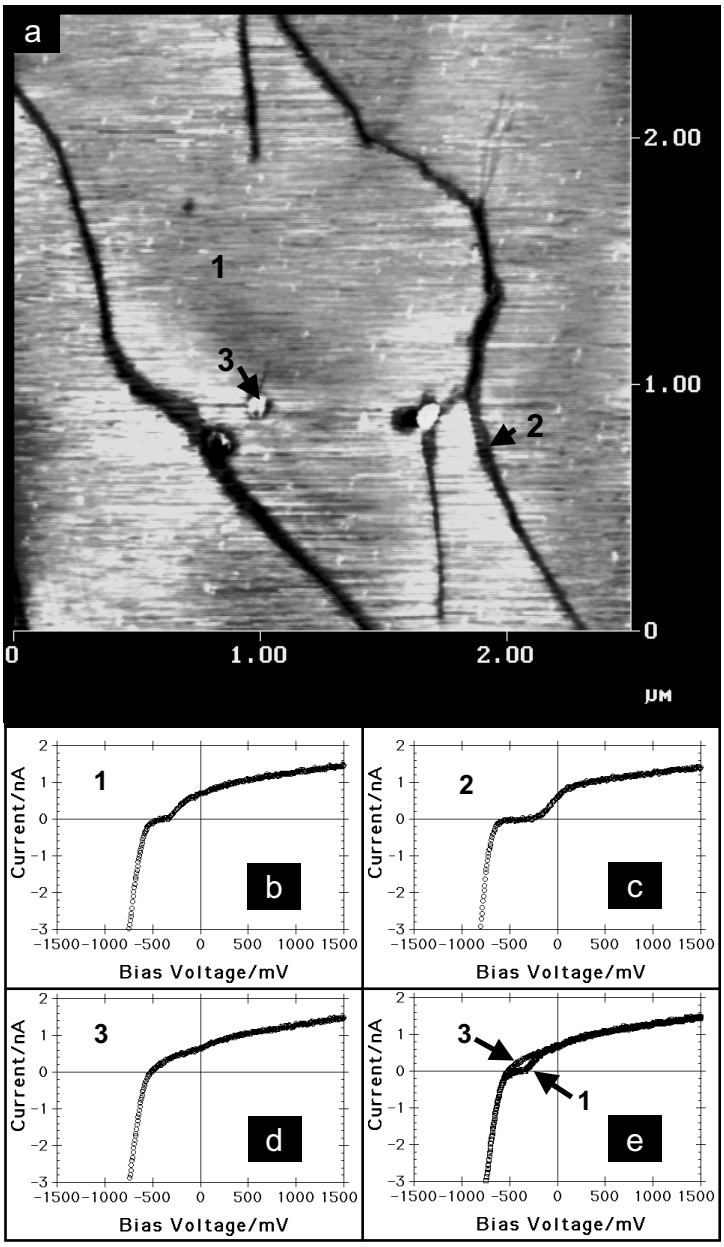
a
1
2
3
2.00
1.00
0
0
1.00
2.00
μm
b
c
d
e
Current/nA
Bias Voltage/mV
-1500 -1000 -500 0 500 1000 1500
2
1
0
-1
-2
-3

Fig. 6

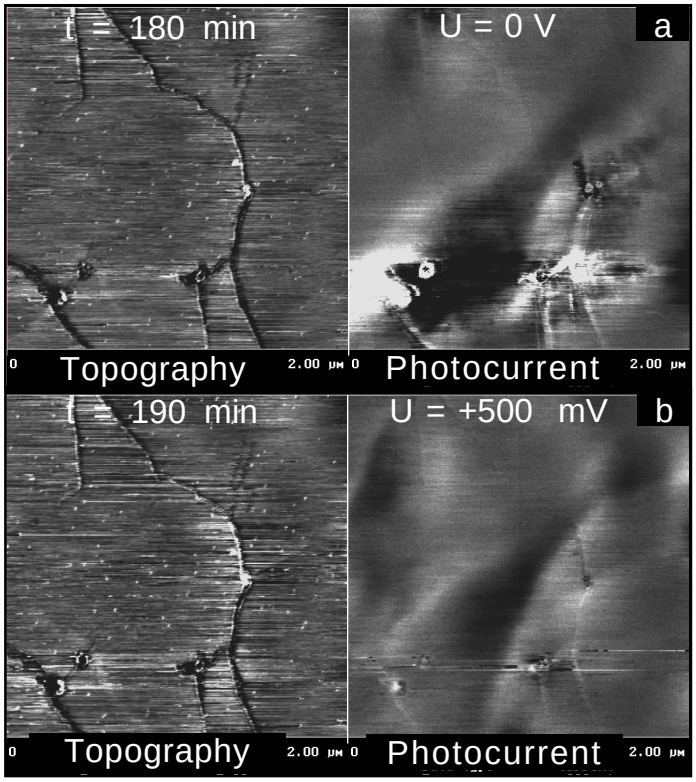
t = 180 min
U = 0 V
a
0
Topography
2.00 µm
0
Photocurrent
2.00 µm
t = 190 min
U = +500 mV
b
0
Topography
2.00 µm
0
Photocurrent
2.00 µm

Fig. 7

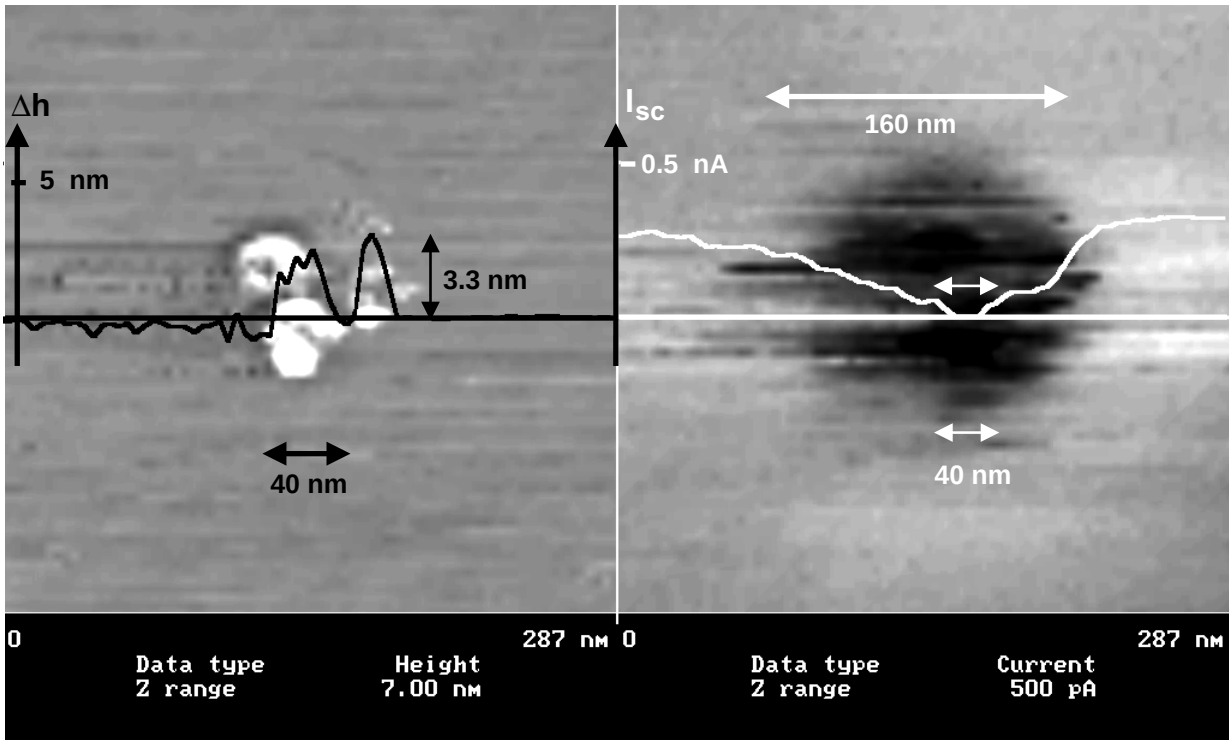
Δh
5 nm
3.3 nm
40 nm
I_{sc}
160 nm
0.5 nA
40 nm
0
287 nm
Data type
Z range
Height
7.00 nm
0
287 nm
Data type
Z range
Current
500 pA

Fig. 8

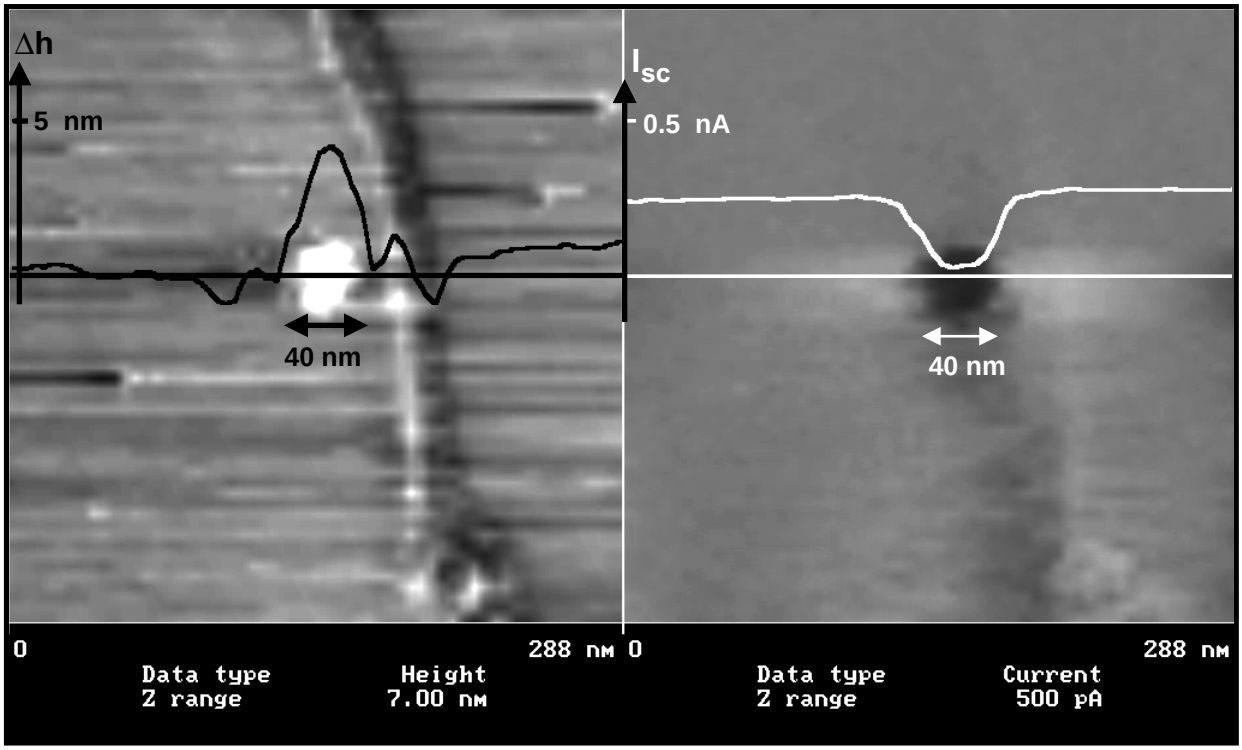
Δh
5 nm
40 nm
I sc
0.5 nA
40 nm
0
288 nm
Data type
Z range
Height
7.00 nm
0
288 nm
Data type
Z range
Current
500 pA

Fig. 9

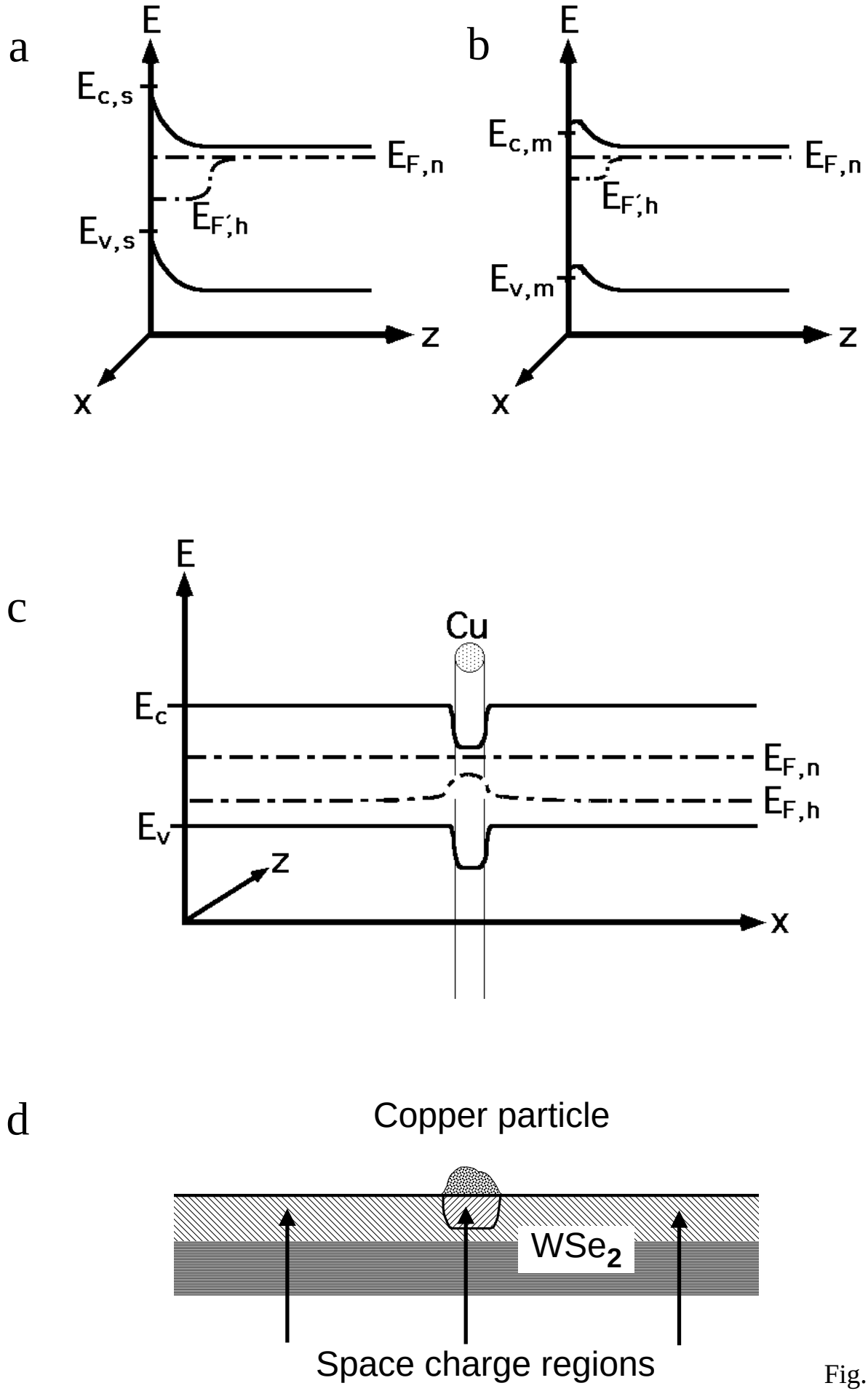
a
E
$E_{c,s}$
$E_{F,n}$
$E_{F',h}$
$E_{v,s}$
z
x
b
E
$E_{c,m}$
$E_{F,n}$
$E_{F',h}$
$E_{v,m}$
z
x
c
E
Cu
E_c
$E_{F,n}$
$E_{F,h}$
E_v
z
x
d
Copper particle
WSe_2
Space charge regions

Fig. 11

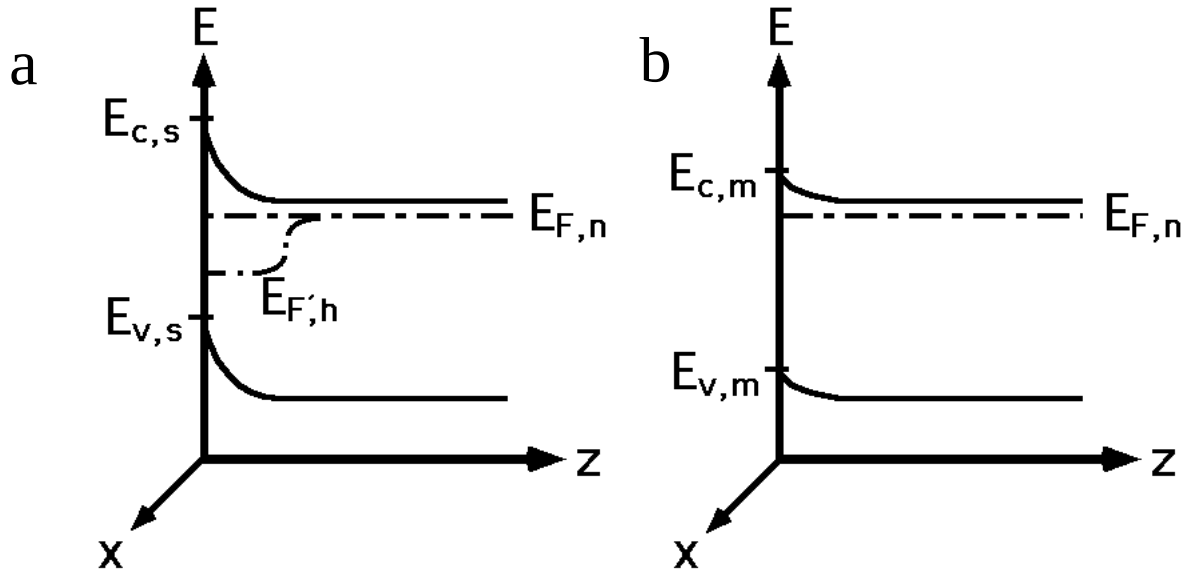
a
E
$E_{c,s}$
$E_{F,n}$
$E_{F',h}$
$E_{v,s}$
z
x
b
E
$E_{c,m}$
$E_{F,n}$
$E_{v,m}$
z
x

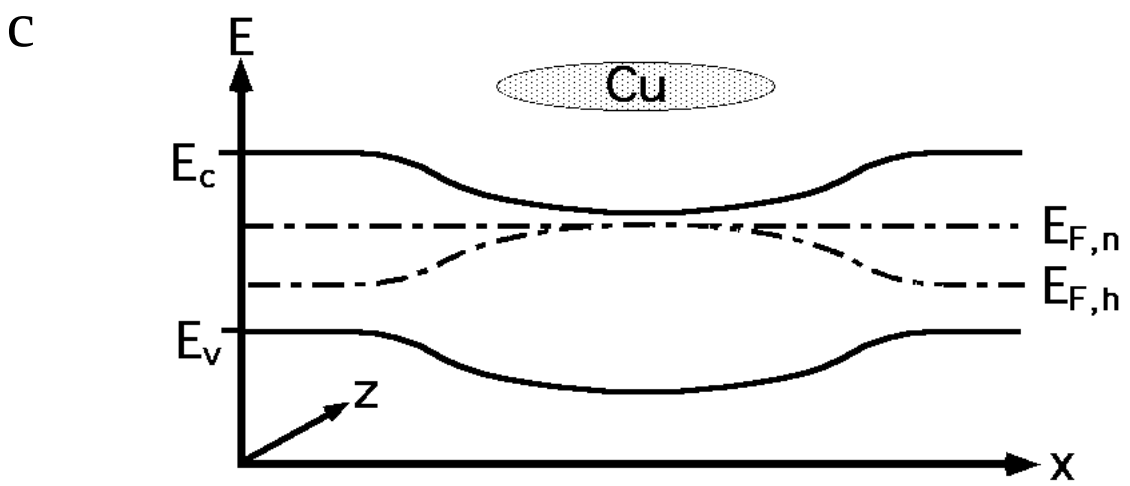
c
E
Cu
E_c
$E_{F,n}$
$E_{F,h}$
E_v
z
x

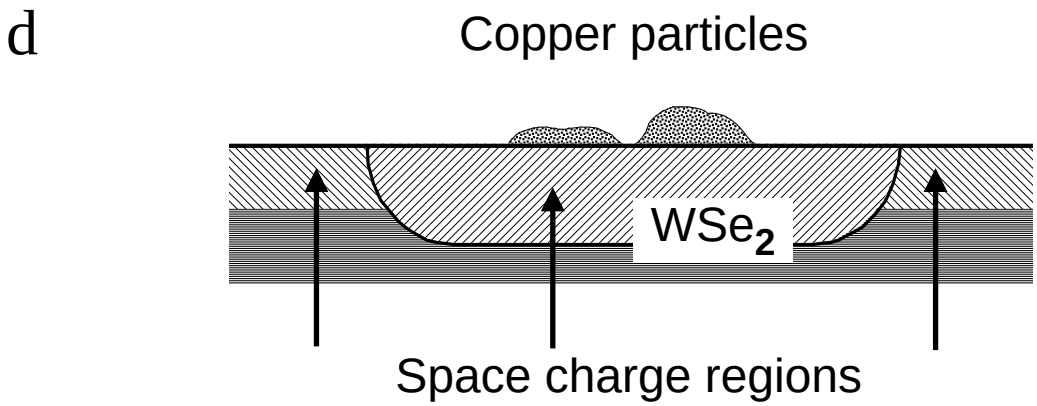
d
Copper particles
WSe_2
Space charge regions

Fig. 10